

Copyright © 1995, by the author(s).  
All rights reserved.

Permission to make digital or hard copies of all or part of this work for personal or classroom use is granted without fee provided that copies are not made or distributed for profit or commercial advantage and that copies bear this notice and the full citation on the first page. To copy otherwise, to republish, to post on servers or to redistribute to lists, requires prior specific permission.

**ROLE OF ETCH PRODUCTS IN POLYSILICON  
ETCHING IN A HIGH DENSITY CHLORINE  
DISCHARGE**

by

C. Lee, D. B. Graves, and M. A. Lieberman

Memorandum No. UCB/ERL M95/9

25 January 1995

COVER 17/1/95

**ROLE OF ETCH PRODUCTS IN POLYSILICON  
ETCHING IN A HIGH DENSITY CHLORINE  
DISCHARGE**

by

C. Lee, D. B. Graves, and M. A. Lieberman

Memorandum No. UCB/ERL M95/9

25 January 1995

**ELECTRONICS RESEARCH LABORATORY**

College of Engineering  
University of California, Berkeley  
94720

**ROLE OF ETCH PRODUCTS IN POLYSILICON  
ETCHING IN A HIGH DENSITY CHLORINE  
DISCHARGE**

by

C. Lee, D. B. Graves, and M. A. Lieberman

Memorandum No. UCB/ERL M95/9

25 January 1995

**ELECTRONICS RESEARCH LABORATORY**

College of Engineering  
University of California, Berkeley  
94720

## Role of Etch Products in Polysilicon Etching in a High Density Chlorine Discharge

C. Lee and D. B. Graves

*Department of Chemical Engineering, University of California, Berkeley, California, 94720*

M. A. Lieberman

*Department of Electrical Engineering and Computer Sciences, University of California, Berkeley, California, 94720*

For low pressure, high density plasma systems, etch products can play a significant role in affecting plasma parameters such as species concentration and electron temperature. The residence time of etch products in the chamber can be long, hence depleting the concentration of the reactants, and leading to a decrease in etch rate. We use a spatially-averaged global model including both gas phase and surface chemistry to study  $\text{Cl}_2$  etching of polysilicon. Etch products leaving the wafer surface are assumed to be  $\text{SiCl}_2$  and  $\text{SiCl}_4$ . These species can be fragmented and ionized by collisions with energetic electrons, generating neutral and charged  $\text{SiCl}_x$  products ( $x = 0 - 4$ ). Two limiting cases of the etch mechanism are found: an ion flux-limited regime and a neutral reactant-limited regime.

The high degree of dissociation in high density plasmas leads to the formation of elemental silicon, which can deposit on the chamber walls and wafer surface. We include surface models for both the wall and the wafer to better understand the role of etch products as a function of flowrate, pressure, and input power. A phenomenological model for the surface chemistry is based on available experimental data. We consider the two limiting conditions of nonreactive and reactive walls. These model perfectly reflective walls, where all silicon-containing species are reflected; and reactive walls, which act as a reactive sites for the formation of  $\text{SiCl}_2$  and  $\text{SiCl}_4$  etch products. The two limiting conditions give significantly different results. A decrease in the absolute atomic silicon density, and a weaker dependence of etch rate on flowrate are observed for the reactive wall.

**Keywords:** Etch Products, nonreactive wall, reactive wall, ion-flux limited, neutral-limited.

## 1. Introduction

Low pressure, high density discharges such as inductively coupled plasma sources have become common for materials etching in the microelectronics industry. Their high etch rate, however, can lead to a build up of etch products in the process chamber and a corresponding depletion of the reactant concentration. As a consequence, high density reactors often require high pumping speed to sweep the etch products out of the chamber. In addition to the depletion of reactants, which decreases the etchant species surface coverage, the presence of etch product species can alter the gas phase composition of both ions and neutrals, and the electron temperature. Several researchers<sup>1,2</sup> have suggested that etch products can be fragmented upon collision with energetic electrons if not removed from the chamber in a relatively short time, with subsequent redeposition on the substrate and chamber walls. Tsujimoto et al<sup>1</sup> found that the etch rate increases by a factor of six when the flowrate is increased from 5 to 100 SCCM.

Due to the relatively high dissociation rate in these high density reactors, for polysilicon etching in a chlorine discharge, the redeposition species can be mainly silicon atoms, which are present in both neutral and ionic form. The elemental silicon, which redeposits onto the chamber wall and wafer surface, can modify surface conditions, affecting the etch rate, uniformity, and other etch properties such as RIE lag, (“aspect-ratio dependent etching”). For example, Dalton and Sawin<sup>3</sup> observed experimentally that RIE lag decreases as the flowrate increases, suggesting that the etch products are removed quickly due to the short residence time, hence minimizing redeposition.

In this work, we address these issues by coupling a gas phase chemistry model that was developed previously<sup>4,5</sup> with a phenomenological surface model. This allows us to investigate the silicon etch rate as a function of power, pressure, and flowrate in the presence of etch products and various reactor wall conditions. The gas phase chemistry model that is used is described in detail in references 4 and 5. In brief, a set of steady state rate equations is written for each species of interest, along with the power balance equation and charge neutrality requirements. The system of equations is solved to obtain species concentrations and electron temperature as a function of input parameters such as power, pressure, and flowrate. The presence of etch products increases the complexity of the system by increasing the number of species, and hence the number of equations. The set of reactions used are listed in Tables I - V. A brief description of the assumptions involved in

obtaining the appropriate cross sections is presented in the next section. We then describe the development and formulation of phenomenological surface models of both the chamber wall and wafer surface, their coupling to the gas phase processes, and the different models for two limiting conditions of reactive and nonreactive reactor walls.

## 2. Model Formulation

### 2.1 Gas Phase Chemistry of Etch Products

For gases such as  $\text{SiCl}_4$  and  $\text{SiCl}_2$ , which appear as the etch products in this model, there is limited information on electron neutral collision cross sections. Hence, we have made estimates based on similar systems. The approach for selecting the appropriate cross sections is systematic: we first look for available cross sections in the tetrachlorosilanes or tetrachloromethanes. If the processes of interest are not available in these systems, we then turn to other halogen containing molecules that have the same tetrahedral structure as  $\text{SiCl}_4$ , such as  $\text{SiF}_4$  and  $\text{CF}_4$ , or chlorine containing compounds that are in the same group as silicon, such as  $\text{CCl}_4$ . For the dissociation reactions of  $\text{SiCl}_x$  ( $x = 1 - 4$ ), we have included all sets of



The rate coefficients for each reaction were based on the cross sectional data for  $\text{SiF}_4$  dissociation<sup>6</sup>. By integrating the cross sections over an assumed Maxwellian distribution, we can obtain analytical expressions for the rate coefficients that have the form of  $k = A \exp(-E_{th}/T_e)$ . The appropriate threshold dissociation energies for the dissociation of  $\text{SiCl}_x$  were adjusted accordingly<sup>7</sup>. The rates for these processes and for the pure chlorine processes are listed in Tables I and IV. The dissociative ionization cross section of  $\text{SiCl}_4$  was based on the ionization data of  $\text{CCl}_4$ <sup>8</sup>, and the ionization of  $\text{SiCl}_4$  to form  $\text{SiCl}_4^+$  was based on the branching ratio for the generation of  $\text{SiCl}_4^+$  and  $\text{SiCl}_3^+$  from  $\text{SiCl}_4$  measured by Coburn<sup>9</sup>. The ionization and partial ionization cross sections for  $\text{SiCl}_3$  were based on data measured by Hayes et al<sup>10</sup> for the  $\text{SiF}_3$  system, and the cross sections for  $\text{SiCl}_2$  were based on the  $\text{SiF}_2$  system measured by Shul et al<sup>11</sup>. For the  $\text{SiCl}$  reactions (11 and 13), we used the set of cross sections for  $\text{GeCl}$ , measured by Shul et al<sup>12</sup>. We did not use the  $\text{SiF}$  cross sections, since collision cross sections for chlorine-containing systems are available. The ionization cross section for  $\text{Si}$  was measured by Freund et al.<sup>14</sup>

Tables II, III, and IV show the reactions used for energy loss of the  $\text{SiCl}_x$  species and the basic chlorine species. The only etch product cross sections available were for  $\text{SiCl}_2$  and  $\text{SiCl}_4$  excitation and momentum transfer processes, calculated by McKoy and co-workers<sup>13</sup>. The vibrational energy loss channels were based on those of  $\text{CCl}_4$ <sup>8</sup>, which were used in the calculation of the energy loss factor  $\epsilon_L$  (see reference 5 for details) for  $\text{SiCl}_4$ ,  $\text{SiCl}_3$ , and  $\text{SiCl}_2$ . These are probably over-estimates since molecules such as  $\text{SiCl}_3$  and  $\text{SiCl}_2$  may have fewer energy loss channels than  $\text{SiCl}_4$ . Nonetheless, they provide a reasonable estimate for the densities of the  $\text{SiCl}_x$  species in the plasma, and can provide qualitative information for a better understanding of systems with complicated plasma chemistry.

## 2.2 Model for Wafer Surface Chemistry

Results of the gas phase model provide quantitative information on energetic ion and neutral fluxes that strike the wafer surface. A phenomenological surface model is needed to obtain the etch rate as a function of these gas phase parameters. This type of model has been developed and used successfully by several researchers<sup>15,16,17</sup>, where first order adsorption kinetics of neutral reactants is observed. The overall etch rate (ER) is a combination of three mechanisms, physical sputtering, ion-enhanced chemical sputtering, and thermal or spontaneous etching.<sup>18,19</sup> In our surface model, we neglect contributions to the total etch rate by physical sputtering and thermal etching. These assumptions are valid for high density sources, where the ion energy is typically between 20 - 50 V, which is only slightly higher than the physical sputtering threshold of polysilicon ( $\sim 20$  V)<sup>15</sup>. The combination of low neutral to ion fluxes and a low surface temperature suggest that the thermal etching component is small.

The etch rate expression is

$$\text{ER} = \frac{Y\theta_{Cl}\Gamma_i}{\rho_{Si}} \quad \text{cm/s} \quad , \quad (1)$$

where the yield  $Y$  is the number of silicon atoms removed per incoming ion,  $\theta_{Cl}$  is the fractional chlorine surface coverage,  $\Gamma_i$  is the total ion flux (# ions /  $\text{cm}^2\text{-s}$ ), and  $\rho_{Si}$  is the solid silicon density ( $6.0 \times 10^{22}$  atoms /  $\text{cm}^3$ ). We assume that the yield is proportional to the square root of ion energy, based on the collision cascade approximation.<sup>20</sup> This has been confirmed recently by Barone and Graves<sup>21</sup> to be valid even for the low energy range, and by Gray et al<sup>15</sup> in their beam study of fluorine etching of silicon. The yield is given

by

$$Y = a \left( E_i^{\frac{1}{2}} - E_{th}^{\frac{1}{2}} \right) \quad , \quad (2)$$

where  $a$  is a parameter,  $E_i$  is the incoming ion energy, which is the sum of the ion energy across the sheath (approximately  $6 T_e$ ) and the bias voltage applied to the wafer holder, and  $E_{th}$  is the threshold energy for ion-enhanced chemical sputtering. This value is approximately 4 eV, based on the work of Gray et al<sup>15</sup>. The significantly lower threshold energy compared to physical sputtering ( $\sim 20$  V) is due to the formation of the chlorosilyl surface layer, in which the Si-Si bonds are weakened because of the “mixing” of chlorine into the silicon surface, hence decreasing the sputtering threshold energy.

The total ion flux  $\Gamma_i$  striking the surface is the sum of all ions present in the plasma,

$$\Gamma_i = \Gamma_{Cl^+} + \Gamma_{Cl_2^+} + \sum_{x=0}^4 \Gamma_{SiCl_x^+} \quad . \quad (3)$$

The ion fluxes are decomposed as  $n_{s,j} \mu_{B,j}$ , where  $n_{s,j}$  is the sheath-edge ion density, and  $\mu_{B,j}$  is the Bohm velocity of ion  $j$ . Details for the calculation of  $n_{s,j}$  from the gas phase particle balance equations can be found in references 4 and 5.

### 2.2.1 Langmuir-Hinshelwood Site Model

The fractional surface coverage  $\theta_{Cl}$  is calculated using a Langmuir-Hinshelwood site model. This method of estimating the halogen surface coverage has been used successfully by many researchers for the study of silicon etching in an ion-assisted environment<sup>22,23,15-17</sup>. In general, the fractional surface coverage can be written as

$$\begin{aligned} \frac{d\theta_{Cl}}{dt} = & \sum_{x=1}^2 (x\Gamma_{Cl_x} S_{Cl_x} + x\Gamma_{Cl_x^+} S_{Cl_x^+}) (1 - \theta_{Cl}) \\ & - (2y_{SiCl_2} + 4y_{SiCl_4}) Y \Gamma_i \theta_{Cl} \quad . \quad (4) \end{aligned}$$

The first term on the right hand side of the equation is the rate of adsorption of chlorine

atoms and molecules onto the silicon wafer, and the second term is the rate of desorption, which is proportional to the removal rate of silicon atoms. The fractions of  $\text{SiCl}_2$  and  $\text{SiCl}_4$  leaving the wafer surface are defined as  $y_{\text{SiCl}_2}$  and  $y_{\text{SiCl}_4}$ , respectively.

The parameters  $S$  used in Eq. (4) are the sticking coefficients of the ions and neutrals, and the  $y$ 's specify the composition of the etch products leaving the wafer surface. For Cl and  $\text{Cl}_2$  neutrals, the sticking coefficients  $S_{\text{Cl}}$  and  $S_{\text{Cl}_2}$  were chosen to be 0.4 and 0.15, respectively. The value of 0.15 was based on the experimental measurements and calculations made by Cheng et al<sup>24</sup> in their investigation of silicon etching by chlorine in a helical resonator discharge. The sticking coefficient of Cl onto Si was chosen to be 0.4 based on the beam study of Kummel and co-workers.<sup>25</sup> Although the study was for a thermal  $\text{Cl}_2$  beam, this gives us a reasonable estimate for thermal Cl adsorption. For the ions  $\text{Cl}^+$  and  $\text{Cl}_2^+$ , the sticking coefficients were assumed to be 0.5. The sticking probability of ions is mainly a function of the ion energy rather than the ion type. This sticking coefficient may be an over-estimate for  $\text{Cl}_2^+$ , since  $\text{Cl}_2^+$  may have a lower sticking coefficient because of mechanisms such as recoil, abstraction, and fragmentation of the ion. Because of the lack of detailed atomistic surface mechanisms, we have assumed that the sticking coefficients for both types of ions are identical. In addition, the molecular species  $\text{Cl}_2$  and  $\text{Cl}_2^+$  are assumed to dissociatively adsorb onto the wafer surface, hence providing two chlorine atoms for surface chlorination. The incoming chlorine neutrals and ions are assumed to adsorb only onto a bare silicon site; hence the  $(1 - \theta_{\text{Cl}})$  term in Eq. (4).

The etch products leaving the surface were assumed to be composed only of  $\text{SiCl}_2$  and  $\text{SiCl}_4$ , as observed experimentally by Coburn<sup>9</sup>, and Rossen and Sawin<sup>26</sup>. The distribution is assumed to be 60%  $\text{SiCl}_2$  and 40%  $\text{SiCl}_4$ , hence giving  $y_{\text{SiCl}_2} = 0.6$  and  $y_{\text{SiCl}_4} = 0.4$ . The term  $(2y_{\text{SiCl}_2} + 4y_{\text{SiCl}_4})$  in Eq. (4) accounts for the actual number of chlorine atoms removed in the form of etch products  $\text{SiCl}_2$  and  $\text{SiCl}_4$ . We have assumed that etching is the only mechanism to remove adsorbed chlorine; other mechanisms such as the sputtering of Cl from the surface are not included in the model. At steady state, the left hand side of Eq. (4) is zero, and  $\theta_{\text{Cl}}$  can be expressed as a function of the fluxes and ion

energy,

$$\theta_{Cl} = \frac{1}{1 + \frac{(2y_{SiCl_2} + 4y_{SiCl_4}) Y \Gamma_i}{\sum_{x=1}^2 x (\Gamma_{Cl_x} S_{Cl_x} + \Gamma_{Cl_x^+} S_{Cl_x^+})}} \quad (5)$$

Note from Eq. (5) that  $\theta_{Cl}$  approaches unity as the ratio of the ion flux  $\Gamma_i$  to the total flux responsible for chlorination ( $\Gamma_{Cl_x} + \Gamma_{Cl_x^+}$ ) becomes small. This is the behavior of first order adsorption kinetics which is described by the Langmuir-Hinshelwood surface model.

### 2.3 Treatment of Chamber Wall Chemistry

In low pressure, high density reactors, the dissociation rate can be relatively high compared to conventional plasma systems. The etch products of  $SiCl_2$  and  $SiCl_4$  leaving the wafer surface will be fragmented and ionized by collisions with energetic electrons to form  $SiCl_x$  components with  $x = 0 - 3$ . Complete dissociation leads to the formation of elemental silicon in both neutral and ionic form,  $Si$  and  $Si^+$ . These silicon species can then redeposit onto the chamber wall and the wafer surface with a high probability, since the deposition process is energetically favorable for elemental  $Si$ . Therefore, we must allow the model to account for different wall conditions and investigate how the wall affects the plasma parameters and the gas phase composition. Since there is limited knowledge about what happens on the reactor wall in the presence of ion bombardment and various incident neutral fluxes, we have chosen to examine two limiting conditions, which we call the non-reactive and reactive wall.

For the nonreactive wall, no silicon containing species is allowed to deposit onto the chamber wall and the wafer surface. The reactor wall is considered to be reflective, such that all silicon-containing ions  $SiCl_x^+$  are neutralized and returned to the gas phase as neutrals, and all silicon-containing neutrals are returned to the gas phase. The chlorine atoms and molecules, on the other hand, are assumed to stick to the wall surface until they passivate the metal wall. Hence, the walls are considered to be coated with a monolayer of chlorine.

For the reactive wall, the chamber wall surface is assumed to act as a reactive site for incoming  $SiCl_x$  and  $Cl$  to generate additional  $SiCl_2$  and  $SiCl_4$ , which are returned to

the gas phase. Since the wall does not have an infinite supply of silicon like the wafer, a different surface model is required to accurately track the presence of silicon and chlorine on the wall surface. The rate of removal, or the wall etch rate, must be a function of both the fractional surface coverage of chlorine and silicon on the wall,  $\theta_{Cl}^w$  and  $\theta_{Si}^w$ , respectively,

$$ER^w = \frac{Y\Gamma_i\theta_{Cl}^w\theta_{Si}^w}{\rho_{Si}} \quad \text{cm/s.} \quad (6)$$

The equations for surface coverage on the reactor wall can be written using the Langmuir-Hinshelwood site model, similar to Eq. (4). For chlorine wall coverage, the general steady state equation becomes

$$\begin{aligned} 0 = & \sum_{x=1}^2 (x\Gamma_{Cl_x} S_{Cl_x}^{metal} + x\Gamma_{Cl_x^+} S_{Cl_x^+}^{metal}) (1 - \theta_{Cl}^w - \theta_{Si}^w) \\ & + \sum_{x=1}^4 (x\Gamma_{SiCl_x} S_{SiCl_x}^{metal} + x\Gamma_{SiCl_x^+} S_{SiCl_x^+}^{metal}) (1 - \theta_{Cl}^w - \theta_{Si}^w) \\ & + \left\{ \sum_{x=1}^4 (x\Gamma_{SiCl_x} S_{SiCl_x}^{Si} + x\Gamma_{SiCl_x^+} S_{SiCl_x^+}^{Si}) + \sum_{x=1}^2 (x\Gamma_{Cl_x} S_{Cl_x}^{Si} + x\Gamma_{Cl_x^+} S_{Cl_x^+}^{Si}) \right\} \theta_{Si}^w \\ & + \left\{ \sum_{x=1}^4 (x\Gamma_{SiCl_x} S_{SiCl_x}^{Cl} + x\Gamma_{SiCl_x^+} S_{SiCl_x^+}^{Cl}) + \sum_{x=1}^2 (x\Gamma_{Cl_x} S_{Cl_x}^{Cl} + x\Gamma_{Cl_x^+} S_{Cl_x^+}^{Cl}) \right\} \theta_{Cl}^w \\ & - (2y_{SiCl_2} + 4y_{SiCl_4}) Y\Gamma_i \theta_{Cl}^w \theta_{Si}^w \end{aligned} \quad (7)$$

The surface coverage expression becomes more complicated since the incoming chlorine-containing fluxes now have the possibility of striking three types of surfaces: metal, chlorine-covered, and silicon-covered. The first two terms in Eq. (7) are the adsorption of chlorine onto a metal surface with the appropriate sticking coefficients. The third term is the adsorption of chlorine on top of a silicon-covered surface, which behaves like the silicon wafer. The fourth term is the adsorption on top of a chlorine-passivated surface, in which the sticking coefficients will be small since the chlorine bonds on the surface are already saturated and any additional species arriving at the surface is unlikely to bond. The last term in the equation is the rate of desorption, or the rate of removal of chlorine in the forms of  $SiCl_2$  and  $SiCl_4$ , which has the same form as Eq. (6). Note that Eq. (7) also

allows for the  $\text{SiCl}_x$  species to contribute to the chlorination of the wall surface. Since Cl can only leave in the forms of  $\text{SiCl}_2$  and  $\text{SiCl}_4$ , the desorption rate is a product of the chlorine and silicon coverages on the wall. Note that in the limit at which either  $\theta_{\text{Cl}}^w$  or  $\theta_{\text{Si}}^w$  goes to zero, there is no formation of  $\text{SiCl}_2/\text{SiCl}_4$  at the wall. Similarly, the steady state equation for the silicon wall coverage can be written as

$$\begin{aligned}
0 = & \sum_{x=0}^4 (\Gamma_{\text{SiCl}_x} S_{\text{SiCl}_x}^{\text{metal}} + \Gamma_{\text{SiCl}_x^+} S_{\text{SiCl}_x^+}^{\text{metal}}) (1 - \theta_{\text{Cl}}^w - \theta_{\text{Si}}^w) \\
& + \left\{ \sum_{x=0}^4 (\Gamma_{\text{SiCl}_x} S_{\text{SiCl}_x}^{\text{Si}} + \Gamma_{\text{SiCl}_x^+} S_{\text{SiCl}_x^+}^{\text{Si}}) \right\} \theta_{\text{Si}}^w \\
& + \left\{ \sum_{x=0}^4 (\Gamma_{\text{SiCl}_x} S_{\text{SiCl}_x}^{\text{Cl}} + \Gamma_{\text{SiCl}_x^+} S_{\text{SiCl}_x^+}^{\text{Cl}}) \right\} \theta_{\text{Cl}}^w \\
& - Y \Gamma_i \theta_{\text{Cl}}^w \theta_{\text{Si}}^w
\end{aligned} \tag{8}$$

Equations (5) - (8) are added to the set of equations for the gas phase concentrations. The system of equations can then be solved to obtain the surface coverage of chlorine and silicon on the chamber wall, and the chlorine surface coverage on the wafer as a function of different operating conditions. Note that Eqs. (7) and (8) are also applicable to the cases of a nonreactive wall if the sticking coefficients of the  $\text{SiCl}_x$  species are set to zero, allowing only Cl and  $\text{Cl}_2$  to stick to the chamber surfaces.

### 2.3.1 Surface Reaction Probabilities

For reaction probabilities on the chamber wall, there are three different types of surfaces that the incoming species see: metal, silicon-passivated metal, and chlorine-passivated metal. The assumed species reaction probabilities with each surface are as follows:

1. Only  $\text{Si}/\text{Si}^+$  and  $\text{SiCl}/\text{SiCl}^+$  are included in the redeposition onto the wafer and chamber surfaces. The bulkier molecules of  $\text{SiCl}_x$  ( $x = 2-4$ ) are assumed to have a smaller reaction probability; hence we neglect such processes.
2. All neutral species of Cl,  $\text{Cl}_2$ , Si, and SiCl that strike the metal surface are assumed to have a sticking coefficient of unity, i.e.,  $S_j^{\text{metal}} = 1$ .
3. For the chlorine-passivated surface, the pure chlorine species of Cl and  $\text{Cl}_2$  have sticking coefficients of zero, i.e.,  $S_{\text{Cl}}^{\text{Cl}} = S_{\text{Cl}_2}^{\text{Cl}} = 0$ ; Si has a sticking coefficient of 0.05,

whereas SiCl sticks with a probability of 0.01. These assumptions are based on the fact that all chlorine bonds are saturated on the surface; therefore, the reaction probability with any incoming Cl and Cl<sub>2</sub> will be low. Silicon and SiCl, however, are energetically favorable to condense on the surface due to their low vapor pressure; hence they will have a finite but small sticking coefficient. No data were found in literature to provide us with reasonable estimates for these numbers, hence, the sticking coefficients are assumed to be factors of 20 or more less than on a metal or silicon-covered surface.

4. For the silicon-passivated surface, Cl and Cl<sub>2</sub> will stick with the same probability as on the wafer surface. Si will have a unity sticking coefficient due to its low vapor pressure, and SiCl will stick with a probability of 0.4, which is lower than Si due to its size and the dependence on which end of the linear molecule arrives at the surface first.
5. All positive ions are assumed to have a sticking coefficient of 0.5, regardless of the surface that they see. The ions that do not stick are returned to the plasma as thermal neutrals.

While the preceding estimates of sticking probabilities seem reasonable, it would be desirable to have better measurements of sticking coefficients for the chlorine-silicon system.

### 3 Results and Discussion

The set of equations for power balance and particle balance for all heavy particle species was solved to obtain the etch rate dependence on different operating conditions of power, pressure, and flowrate. The results are presented in two separate sections of nonreactive and reactive walls. We will also compare and contrast the differences in the results for the two limiting conditions, concentrating on how the etch rate and gas phase composition are affected by the assumptions on the wall conditions. Figure 1 shows a schematic of the reactor configuration used in the model. The reactor geometry was based on a commercially available transformer-coupled-plasma (TCP) reactor, with  $R = 15.25$  cm and  $L = 7.5$  cm. Feed gas flows into the reactor as pure Cl<sub>2</sub>. Upon fragmentation and ionization, reactive species of Cl, Cl<sup>+</sup>, and Cl<sub>2</sub><sup>+</sup> are generated. These species react with the silicon wafer, forming etch products SiCl<sub>2</sub> and SiCl<sub>4</sub>, which return to the gas phase. The etch products are fragmented and ionized to other components by collisions with energetic electrons. As a result, the plasma consists of neutrals Cl<sub>2</sub>, Cl, SiCl<sub>x</sub> ( $x = 0-4$ ), positive ions Cl<sub>2</sub><sup>+</sup>, Cl<sup>+</sup>, SiCl<sub>x</sub><sup>+</sup>, and negatively charged Cl<sup>-</sup> and e<sup>-</sup>.

#### 3.1 Nonreactive Wall

As discussed in section 2.2, for the nonreactive wall, the walls are passivated with chlorine and are perfectly reflective to all the silicon-containing species. The surface recombination coefficient of chlorine on the wall is assumed to be 0.1; i.e., the recombination probability of Cl to form  $\text{Cl}_2$  is 10%. No redeposition of silicon was included in this case, and all neutrals of  $\text{SiCl}_x$  bounce back, whereas  $\text{SiCl}_x^+$  is neutralized on the wall and returned to the gas phase as  $\text{SiCl}_x$ . All the results shown have a constant DC bias of -30 V on the wafer holder, which means that the ion energy is the sum of the plasma potential (approximately 15 - 20 V) and 30 V.

Figure 2 shows the etch rate as a function of flowrate  $Q$ , with the coil power as the parameter, at a reactor pressure of 1 mTorr. Since the reactor pressure is defined as  $p = \sum n_i kT$ , where  $\sum n_i$  is the sum of all neutral densities in the plasma, the reactor pressure is affected by the amount of etch products present. The variation in etch rate due to a change in power depends on flowrate. In the low flowrate regime, increasing the power does not affect the etch rate much, whereas at higher flowrates, increasing power can significantly increase the etch rate. In the low flowrate range, the etch rate is surface coverage (Cl) limited; hence increasing the power has little effect on the etch rate. As the surface becomes saturated, which is the high flowrate regime, the etch rate is limited by the ion flux striking the surface. As seen in Figure 2, for  $Q$  greater than about 20 SCCM, increasing the power from 500 W to 2000 W increases the etch rate by almost a factor of three. At constant power, the etch rate dependence on flowrate directly follows the first order adsorption kinetics. In the low flowrate range, the increase in flowrate increases the etch rate rapidly due to the increase in the halogen surface coverage. As the surface becomes saturated with chlorine, increasing the flowrate no longer increases the etch rate, and the final result is an etch rate of constant value as flowrate increases. The solid dots in Figure 2 are experimental data measured by Tsujimoto et al<sup>10</sup> in a study of Si etching by  $\text{Cl}_2$ . The data were scaled to fit onto the graph since the etch rate calculated by the model is only accurate in the qualitative sense. Therefore, we did not attempt to make quantitative comparisons. From Figure 2, we see that the qualitative trends of etch rate versus  $Q$  agree fairly well with our model predictions.

Figure 3 shows a plot of the fractional etch product versus  $Q$ , for the same parameters as Figure 2. The fractional etch product is defined as the sum of all  $\text{SiCl}_x$  densities divided by the total neutral density. A high fraction means that the  $\text{SiCl}_x$  concentration in the gas phase is high, and the reactant supply is depleted. In the low flowrate range, the fractional etch product is in excess of 0.6, suggesting that in this range, the etch products are not pumped out fast enough. The residence time  $\tau$  is  $pV/Q$ , where  $p$  is the reactor pressure, and  $V$  is the reactor volume. As the flowrate increases,  $\tau$  decreases, and the fractional etch product drops to less than 0.1 at a flowrate of 100 SCCM. The accumulation of etch

products in the low Q range corresponds to the low etch rate shown in Figure 2, suggesting that the presence of etch products depletes the reactant supply. This decreases the halogen surface coverage, and the etch rate decreases as a result. In the high flowrate range, the etch products are removed relatively fast from the chamber, and the etch rate increases. An increase in power also increases the fractional etch product in the gas phase. This is due to the higher silicon etch rate, leading to a higher concentration of silicon containing species in the discharge for the same residence time.

In order to verify that the etch rate is indeed ion flux limited in the high flowrate range, we plot in Figure 4 the fractional halogen surface coverage  $\theta_{Cl}$  versus Q, with power as a parameter. As the power increases, we see that  $\theta_{Cl}$  decreases at a fixed Q. This is opposite to the trend of the etch rate dependence on power in the high flowrate range as shown in Figure 2. Therefore, it is confirmed that in this region, the etch rate is not controlled by the surface coverage, but rather by the ion flux. The decrease in  $\theta_{Cl}$  as power increases is due to the increase in the total ion flux. As the ion flux increases, the rate of desorption of Cl on the surface increases, since the removal rate is proportional to  $\Gamma_i$ , hence decreasing the steady state chlorine surface coverage.

Figure 5 shows the etch rate dependence on pressure, with flowrate as a parameter. At a fixed power of 1000 W, the etch rate behavior shows two different trends, depending on the flow into the system. For a low flowrate of 4 SCCM, the polysilicon etch rate increases steadily as pressure is increased from 1 to 20 mTorr. This is due to an increase of the halogen surface coverage as pressure is increased. In this reactant supply limited regime, the etch rate increases as the halogen surface coverage increases. In the high flowrate range, the etch rate shows a different trend. As pressure increases, the etch rate peaks at approximately 7 mTorr and then drops off at higher pressures. This suggests that at high pressures, the etch rate follows the trends of the ion flux, hence corresponding to observations shown in Figure 2 that the etch mechanism is ion flux limited in the high flowrate regime. If we plot the ion flux versus pressure, we would see that for all three flowrates, the ion flux decreases as pressure increases due to a decrease in both  $T_e$  and total  $n^+$ . The etch rate, however, will only follow this trend in the high flowrate regime. In addition, Figure 5 shows that the etch rate at 50 SCCM is higher than 100 SCCM for a fixed pressure. This is due to a decrease in the total ion flux as flowrate increases. The decrease is due to a lower concentration of Si in the gas phase. Since Cl has an ionization potential 5.5 eV higher than Si, the ion density is lower for the same power input at high flowrates.

### 3.2 Reactive Wall

For the reactive wall, the chamber wall surface acts as a reactive site that can gen-

erate  $\text{SiCl}_2$  and  $\text{SiCl}_4$ , as shown in Figure 6. In this case, Si and SiCl neutrals and ions are allowed to deposit onto both the wafer and wall surfaces. The fractional surface coverages of silicon and chlorine  $\theta_{\text{Cl}}^w$  and  $\theta_{\text{Si}}^w$  on the wall are determined as described in Section 2.3. Knowing  $\theta_{\text{Cl}}^w$  and  $\theta_{\text{Si}}^w$  allows us to calculate how much etch products are formed from the wall and recycled back into the process chamber. Effectively, this provides an additional loss process for species of Si and SiCl, and as we shall see from the results, the gas phase composition and etch rate behavior in this limiting condition are different from the nonreactive wall condition.

Figure 7 shows a comparison between etch rates for the nonreactive and reactive walls. Operating conditions are identical, both at a pressure of 1 mTorr and coil power of 1000 W. The etch rate for the reactive wall shows a weaker dependence on flowrate, suggesting that the dilution effect is not as important. This is due to the additional loss process for silicon to the wall, where the returned  $\text{SiCl}_x$  product is either  $\text{SiCl}_2$  or  $\text{SiCl}_4$ . This reduces the fraction of elemental Si in the gas phase. For time scales at which the silicon loss rate to the wall is faster than the pumping loss, the dilution effect is not as important. For the nonreactive wall, there is no wall loss for Si, hence the pumping loss plays a large role. The lower etch rate for the reactive wall is due to the decrease in the total ion flux that strikes the wafer. This decrease is due to the decrease in the fraction of Si in the discharge, which leads to a lower total ion flux since elemental silicon is easier to ionize than chlorine.

The weaker dependence of etch rate on flowrate for the reactive wall in Fig. 7 is also due to the lower fractional etch product in the gas phase. Recall that in the low flowrate regime, the etch mechanism is reactant supply limited. If the fraction of etch products in the gas phase is low at the same reactor pressure, then the reactant supply is no longer limited and the dilution effect is less dominant. Hence increasing the flowrate will not affect the etch rate to a great extent. Figure 8 shows the difference in the fractional etch product in the gas phase for the two wall conditions. There is a drastic difference, especially in the flowrate ranges of 4 - 40 SCCM. At the lowest flow, or the longest residence time, etch product accumulation for the nonreactive wall is in excess of 70%, whereas for the reactive wall, the fraction of etch products is only 20%. The reason for this is that when the chamber walls are reactive, they can serve as active sites for heterogeneous reactions to take place. Under these conditions, more  $\text{SiCl}_2$  and  $\text{SiCl}_4$  are formed at the expense of Si, hence decreasing the absolute number density of Si. This leads to a decrease in the total neutral density of silicon containing species. Since the reactor pressure depends on the total neutral density, a significant decrease in Si density will lead to a decrease in reactor pressure. In order to maintain a constant reactor pressure of 1 mTorr, more  $\text{Cl}_2$  can flow into the system, in effect increasing the chlorine densities, and the frac-

tional etch product goes down.

Redeposition of etch products can also be significant in these high density discharges, especially if they are not removed promptly. This could lead to poor etch uniformity, microloading effects, and lower etch rates. Since redeposition by both ions and neutrals is possible, one would be interested to know which type of redeposition is dominant. Figure 9 shows the total etch rate, net etch rate, and the deposition rates of ions and neutrals as a function of flowrate. The total redeposition rate can be as high as  $800 \text{ \AA}/\text{min}$  at the lowest flowrate. We observe that redeposition is mainly due to ions rather than neutrals. One might suggest that this is strictly an artifact of the assumptions used for sticking coefficients. However, for energetic ions with energies in the range of 20 - 50 eV, the reaction probability of ions sticking to a surface is only weakly dependent on surface coverage. The neutrals, on the other hand, can only redeposit onto a bare silicon site. If the surface is covered with chlorine, then the redeposition due to neutrals is much lower, even if the neutrals have higher sticking probabilities than ions, since the effective neutral sticking coefficient  $\propto S(1 - \theta_{Cl})$  decreases linearly with increasing surface coverage.

The gas phase composition is also affected by the wall conditions, especially the concentration of elemental silicon. Figures 10a and 10b show the difference in the neutral densities for the two different wall conditions, both at a reactor pressure of 1 mTorr and power of 1000 W. For the nonreactive wall of Fig. 10a, the dominant neutral species are Cl, Cl<sub>2</sub>, and Si, with elemental Si density exceeding the Cl density at low flowrates. All other SiCl<sub>x</sub> species concentrations are an order of magnitude lower and hence are unimportant. Once the reactor walls are allowed to be reactive, the Si density significantly drops, as shown in Fig. 10b. The dominant neutrals are still Cl and Cl<sub>2</sub>, but the elemental silicon concentration has dropped by two orders of magnitude compared to the nonreactive wall case. All other SiCl<sub>x</sub> densities are higher, due to the enhanced reactivity on the wall to form more SiCl<sub>2</sub> and SiCl<sub>4</sub>. These densities are still much lower than the chlorine densities, which explains why the fractional etch products for the reactive wall are lower, as seen in Fig. 8.

#### 4. Conclusions

We have developed a gas phase model that includes the etch products for Cl<sub>2</sub> etching of silicon in a high density discharge. The reactive processes that take place in the plasma were coupled to the surfaces of the silicon wafer and the chamber walls through phenomenological surface models. Since the degree of uncertainty associated with the surface model of the reactor walls is large, we have taken the approach of examining two limiting wall conditions. For the nonreactive wall, the surface is essentially a perfect

reflector for all silicon-containing species, whereas for the reactive wall, the incoming Si and SiCl neutrals and ions are allowed to react with Cl to form SiCl<sub>2</sub> and SiCl<sub>4</sub>.

From the model results, we found using the assumption of a Langmuir-Hinshelwood adsorption isotherm that the etch rate has first-order adsorption kinetics at a constant power and pressure. Further investigations of etch rate dependence on flowrate, power, and pressure have identified two etch regimes: halogen surface-coverage-limited and ion flux-limited. In the surface-coverage-limited regime, etch rate increases with increasing pressure and flowrate, and there is a weak dependence on power. In the ion flux-limited regime, etch rate is a strong function of power. Increasing the pressure or the flowrate in this regime will have minimal effect on the etch rate.

The assumptions on the reactivity of the reactor wall lead to different behaviors in the etch rate and gas phase composition. The fractional etch product in the gas phase was observed to be lower when the walls are assumed to be reactive, since the Si and SiCl species were allowed to redeposit onto the chamber wall and react to form gas phase SiCl<sub>2</sub> and SiCl<sub>4</sub>. In addition, elemental silicon is no longer the dominant SiCl<sub>x</sub> species. The etch rate dependence on flowrate was weaker when the reactor wall was reactive, since pumping loss is no longer the dominant loss mechanism for Si, but rather, wall losses also play an important role.

The model has also accounted for redeposition of the etch products back onto the wafer surface. By comparing the deposition rates of both ions and neutrals, we have found that the dominant depositing species are the ions. Unfortunately, there are no experimental data to confirm this finding of the model.

Table I. Chlorine Reaction Set\*

Reaction	Rate Coefficients
e + Cl <sub>2</sub> → Cl <sub>2</sub> <sup>+</sup> + 2e	$k = 9.21 \times 10^{-8} \exp(-12.9 / T_e) \text{ cm}^3 \text{ s}^{-1}$
e + Cl <sub>2</sub> → Cl <sup>+</sup> + Cl + 2e	$k = 3.88 \times 10^{-9} \exp(-15.5 / T_e) \text{ cm}^3 \text{ s}^{-1}$
e + Cl <sub>2</sub> → Cl <sup>+</sup> + Cl + e	$k = 8.55 \times 10^{-10} \exp(-12.65 / T_e) \text{ cm}^3 \text{ s}^{-1}$
e + Cl <sub>2</sub> → 2Cl( <sup>2</sup> P) + e	$k = 3.80 \times 10^{-8} \exp(-3.824 / T_e) \text{ cm}^3 \text{ s}^{-1}$
e + Cl <sub>2</sub> → Cl( <sup>2</sup> P) + Cl <sup>+</sup>	$k = 3.69 \times 10^{-10} \exp(-1.68 / T_e + 1.457 / T_e^2 - 0.44 / T_e^3 + 0.0572 / T_e^4 - 0.0026 / T_e^5) \text{ cm}^3 \text{ s}^{-1}$
e + Cl( <sup>2</sup> P) → Cl <sup>+</sup> + 2e	$k = (T_e / 12.96)^{0.5} \exp(-12.96 / T_e) (1.419 \times 10^{-7} - 1.864 \times 10^{-8} \log(T_e / 12.96) - 5.439 \times 10^{-8} \log(T_e / 12.96)^2 + 3.306 \times 10^{-8} \log(T_e / 12.96)^3 - 3.54 \times 10^{-9} \log(T_e / 12.96)^4 - 2.915 \times 10^{-8} \log(T_e / 12.96)^5) \text{ cm}^3 \text{ s}^{-1}$
Cl <sup>+</sup> + Cl <sub>2</sub> <sup>+</sup> → Cl( <sup>2</sup> P) + Cl <sub>2</sub>	$k = 5.0 \times 10^{-8} \text{ cm}^3 \text{ s}^{-1}$
Cl <sup>+</sup> + Cl <sup>+</sup> → Cl( <sup>2</sup> P) + Cl( <sup>2</sup> P <sub>u</sub> )	$k = 5.0 \times 10^{-8} \text{ cm}^3 \text{ s}^{-1}$
e + Cl <sup>+</sup> → Cl( <sup>2</sup> P) + 2e	$k = 2.63 \times 10^{-8} \exp(-5.37 / T_e) \text{ cm}^3 \text{ s}^{-1}$
Cl( <sup>2</sup> P) → 1/2 Cl <sub>2</sub>	$k = \gamma_{rec} D_{eff} / \Lambda^2 \text{ s}^{-1}$
Cl <sup>+</sup> → Cl( <sup>2</sup> P)	$k = 2\mu_{B,Cl^+} (R^2 h_L + RLh_R) / R^2 L \text{ s}^{-1}$
Cl <sub>2</sub> <sup>+</sup> → Cl <sub>2</sub> (g)	$k = 2\mu_{B,Cl_2^+} (R^2 h_L + RLh_R) / R^2 L \text{ s}^{-1}$
$T_e$ [=] eV	

\* See Reference 5 for details.

Table II. Energy Loss Reactions for Chlorine Molecules\*

Reaction	Rate Coefficient
$e + \text{Cl}_2 \longrightarrow \text{Cl}_2 (b^3\Pi_u) + e$	$k = 6.13 \times 10^{-10} \exp(2.74 / T_e - 6.85 / T_e^2 + 3.69 / T_e^3 - 0.856 / T_e^4 + 0.0711 / T_e^5) \text{ cm}^3 \cdot \text{s}^{-1}$
$\longrightarrow \text{Cl}_2 ({}^1\Pi_u) + e$	$k = 3.80 \times 10^{-8} \exp(-3.824 / T_e) \text{ cm}^3 \cdot \text{s}^{-1}$
$\longrightarrow \text{Cl}_2 ({}^1\Pi_g) + e$	$k = 9.74 \times 10^{-9} \exp(-10.71 / T_e) \text{ cm}^3 \cdot \text{s}^{-1}$
$\longrightarrow \text{Cl}_2 ({}^1\Sigma_u) + e$	$k = 2.12 \times 10^{-9} \exp(-11.16 / T_e) \text{ cm}^3 \cdot \text{s}^{-1}$
$\longrightarrow \text{Cl}_2 + e$	$k = 4.47 \times 10^{-7} \exp(-2.17 / T_e + 0.362 / T_e^2 - 0.0196 / T_e^3) \text{ cm}^3 \cdot \text{s}^{-1}$ (momentum transfer)
$\longrightarrow \text{Cl}_2^+ + e$	$k = 9.21 \times 10^{-8} \exp(-12.9 / T_e) \text{ cm}^3 \cdot \text{s}^{-1}$
$\longrightarrow \text{Cl}_2 + e$	$k = 9.26 \times 10^{-10} \exp(5.85 / T_e - 4.94 / T_e^2 + 1.716 / T_e^3 - 0.251 / T_e^4 + 0.123 / T_e^5) \text{ cm}^3 \cdot \text{s}^{-1}$ (vibrational excitation)
$\longrightarrow 2\text{Cl} ({}^2\text{P}) + e$	$k = 3.80 \times 10^{-8} \exp(-3.824 / T_e) \text{ cm}^3 \cdot \text{s}^{-1}$

\* See Reference 5 for details.

Table III. Energy Loss Reactions for Chlorine Atoms\*

Reaction	Process
$e + \text{Cl}(^2\text{P}) \longrightarrow \text{Cl}(^3\text{D}) + 2e$	$k = 1.99 \times 10^{-8} \exp(-10.06 / T_e) \text{ cm}^3 \cdot \text{s}^{-1}$
$\longrightarrow \text{Cl}(^4\text{D}) + e$	$k = 9.24 \times 10^{-9} \exp(-11.15 / T_e) \text{ cm}^3 \cdot \text{s}^{-1}$
$\longrightarrow \text{Cl}(^4\text{P}) + e$	$k = 1.60 \times 10^{-8} \exp(-10.29 / T_e) \text{ cm}^3 \cdot \text{s}^{-1}$
$\longrightarrow \text{Cl}(^4\text{S}) + e$	$k = 1.27 \times 10^{-8} \exp(-10.97 / T_e) \text{ cm}^3 \cdot \text{s}^{-1}$
$\longrightarrow \text{Cl}(^5\text{D}) + e$	$k = 5.22 \times 10^{-9} \exp(-11.12 / T_e) \text{ cm}^3 \cdot \text{s}^{-1}$
$\longrightarrow \text{Cl}(^5\text{P}) + e$	$k = 2.79 \times 10^{-9} \exp(-11.06 / T_e) \text{ cm}^3 \cdot \text{s}^{-1}$

\* See Reference 5 for details.

Table IV. Etch Product Reaction Set\*

Reaction	Rate Coefficients
e + SiCl <sub>4</sub>	$k_1 = 7.03 \times 10^{-8} \exp(-12.44 / T_e) \text{ cm}^3 \text{ s}^{-1}$
e + SiCl <sub>4</sub>	$k_2 = 7.27 \times 10^{-9} \exp(-4.73 / T_e) \text{ cm}^3 \text{ s}^{-1}$
e + SiCl <sub>4</sub>	$k_3 = 2.0 \times 10^{-7} \exp(-12.44 / T_e) \text{ cm}^3 \text{ s}^{-1}$
e + SiCl <sub>3</sub>	$k_4 = 1.68 \times 10^{-8} \exp(-7.65 / T_e) \text{ cm}^3 \text{ s}^{-1}$
e + SiCl <sub>3</sub>	$k_5 = 7.27 \times 10^{-9} \exp(-2.91 / T_e) \text{ cm}^3 \text{ s}^{-1}$
e + SiCl <sub>3</sub>	$k_6 = 4.90 \times 10^{-8} \exp(-13.9 / T_e + 6.89 / T_e^2 - 1.45 / T_e^3) \text{ cm}^3 \text{ s}^{-1}$
e + SiCl <sub>3</sub>	$k_7 = 2.41 \times 10^{-8} \exp(-14.75 / T_e + 2.504 / T_e^2) \text{ cm}^3 \text{ s}^{-1}$
e + SiCl <sub>2</sub>	$k_8 = 7.27 \times 10^{-9} \exp(-4.99 / T_e) \text{ cm}^3 \text{ s}^{-1}$
e + SiCl <sub>2</sub>	$k_9 = 2.98 \times 10^{-8} \exp(-9.81 / T_e) \text{ cm}^3 \text{ s}^{-1}$
e + SiCl <sub>2</sub>	$k_{10} = 8.93 \times 10^{-8} \exp(-9.81 / T_e) \text{ cm}^3 \text{ s}^{-1}$
e + SiCl	$k_{11} = 7.54 \times 10^{-8} \exp(-6.79 / T_e) \text{ cm}^3 \text{ s}^{-1}$
e + SiCl	$k_{12} = 7.27 \times 10^{-9} \exp(-3.95 / T_e) \text{ cm}^3 \text{ s}^{-1}$
e + SiCl	$k_{13} = 8.85 \times 10^{-8} \exp(-12.1 / T_e) \text{ cm}^3 \text{ s}^{-1}$
e + Si	$k_{14} = 7.85 \times 10^{-8} \exp(-7.41 / T_e) \text{ cm}^3 \text{ s}^{-1}$
SiCl <sub>x</sub> <sup>+</sup> + Cl <sup>-</sup>	$k_{15} = 5.0 \times 10^{-8} \text{ cm}^3 \text{ s}^{-1}$
SiCl <sub>x</sub> <sup>+</sup>	$k_{16} = 2u_{Bj}(R^2 h_L + RLh_R) / R^2 L \text{ s}^{-1}(\dagger)$
T <sub>e</sub> [=] eV	

\*See text for references.

†See reference 5 for details;  $u_{Bj}$  is the Bohm velocity of the respective positive ions.

Table V. Energy Loss Reactions for SiCl<sub>x</sub> Molecules\*

Reaction	Rate Coefficient
e + SiCl <sub>4</sub>	
----->	SiCl <sub>4</sub> (v = 1) + e
	$k = 3.68 \times 10^{-9} \exp(2.72 / T_e - 1.91 / T_e^2 + 0.638 / T_e^3 - 0.9 / T_e^4 + 0.0045 / T_e^5) \text{ cm}^3 \cdot \text{s}^{-1}$
----->	SiCl <sub>4</sub> (v = 2) + e
	$k = 2.42 \times 10^{-9} \exp(-2.65 / T_e + 2.12 / T_e^2 - 0.715 / T_e^3 - 0.103 / T_e^4 - 0.005 / T_e^5) \text{ cm}^3 \cdot \text{s}^{-1}$
----->	SiCl <sub>4</sub> (v = 3) + e
	$k = 4.48 \times 10^{-8} \exp(2.64 / T_e - 2.17 / T_e^2 + 0.765 / T_e^3 - 0.11 / T_e^4 + 0.0056 / T_e^5) \text{ cm}^3 \cdot \text{s}^{-1}$
----->	SiCl <sub>4</sub> (v = 4) + e
	$k = 2.00 \times 10^{-9} \exp(2.02 / T_e - 1.07 / T_e^2 - 0.29 / T_e^3 - 0.037 / T_e^4 + 0.0016 / T_e^5) \text{ cm}^3 \cdot \text{s}^{-1}$
----->	SiCl <sub>4</sub> * + e
	$k = 3.21 \times 10^{-7} \exp(-8.27 / T_e) \text{ cm}^3 \cdot \text{s}^{-1}$ (excitation)
----->	SiCl <sub>4</sub> + e
	$k = 6.30 \times 10^{-8} \exp(1.58 / T_e - 1.687 / T_e^2 + 0.61 / T_e^3 - 0.091 / T_e^4 + 0.0045 / T_e^5) \text{ cm}^3 \cdot \text{s}^{-1}$ (momentum transfer)
e + SiCl <sub>2</sub>	
----->	SiCl <sub>2</sub> *(a <sup>3</sup> B1) + e
	$k = 1.72 \times 10^{-8} \exp(-2.12 / T_e - 0.08 / T_e^2 + 0.0057 / T_e^3) \text{ cm}^3 \cdot \text{s}^{-1}$
----->	SiCl <sub>2</sub> *(A <sup>1</sup> B1) + e
	$k = 3.71 \times 10^{-8} \exp(-5.604 / T_e) \text{ cm}^3 \cdot \text{s}^{-1}$
----->	SiCl <sub>2</sub> + e
	$k = 5.00 \times 10^{-7} \exp(-2.34 / T_e - 0.94 / T_e^2 - 0.169 / T_e^3 + 0.0092 / T_e^4) \text{ cm}^3 \cdot \text{s}^{-1}$ (momentum transfer)

\* See text for references.

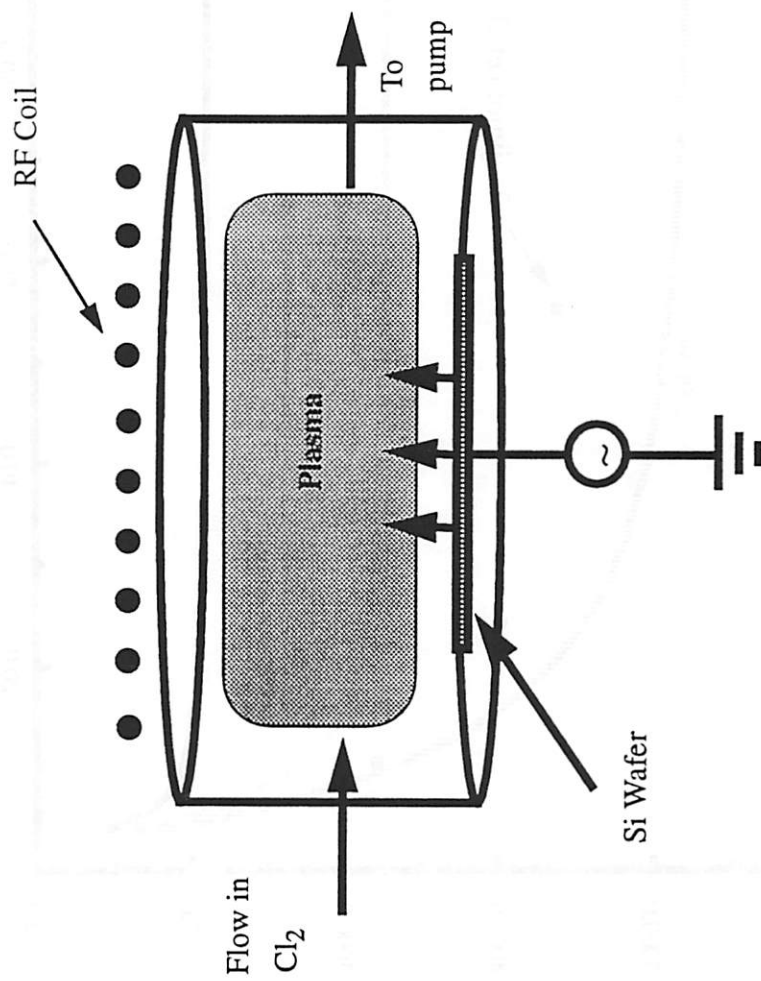


Figure 1. Reactor configuration used in the formulation, with  $R = 15.25$  cm, and  $L = 7.5$  cm.

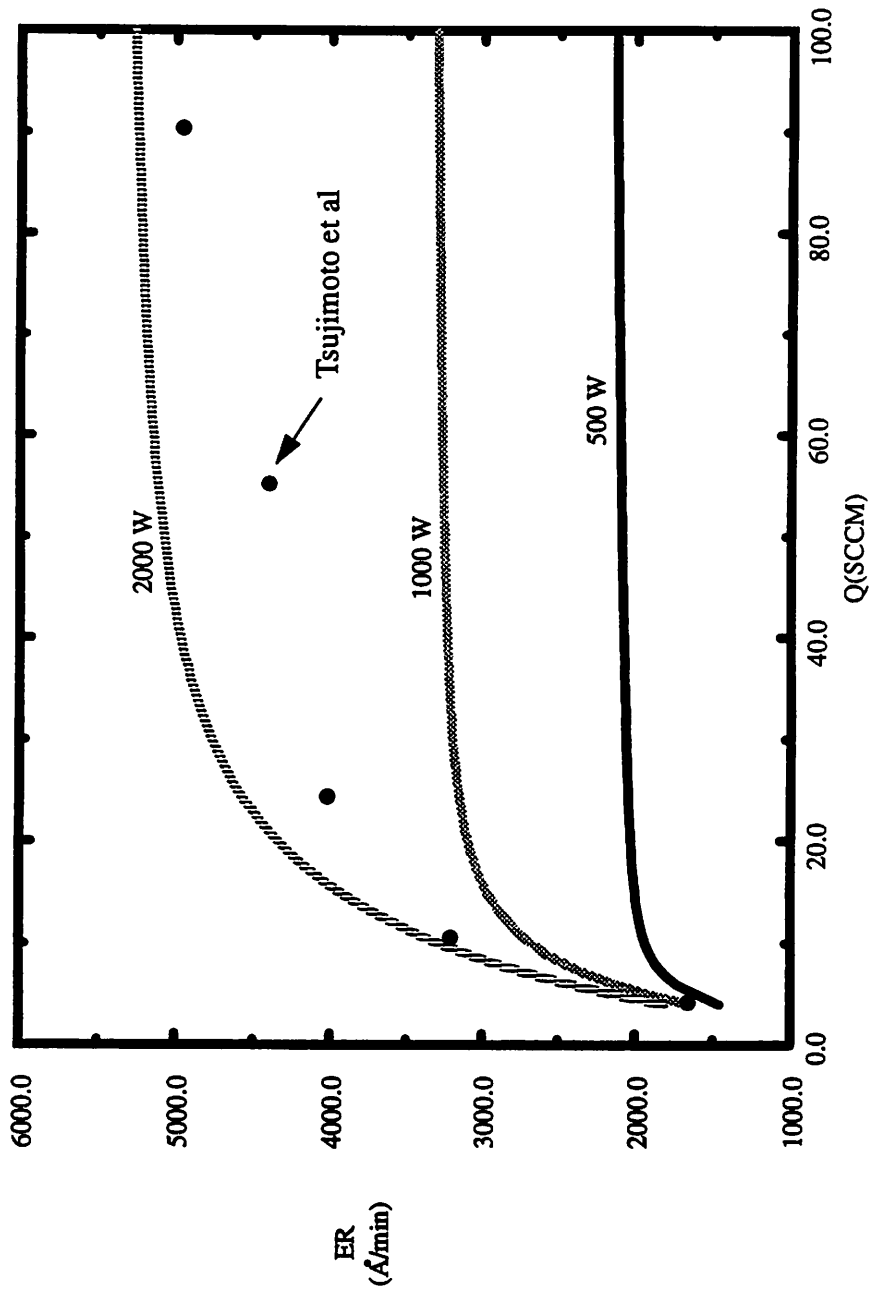


Figure 2. Polysilicon etch rate vs. flowrate, nonreactive wall case, pressure = 1m Torr, coil power is the parameter. Solid dots are experimental data measured by Tsujimoto et al.

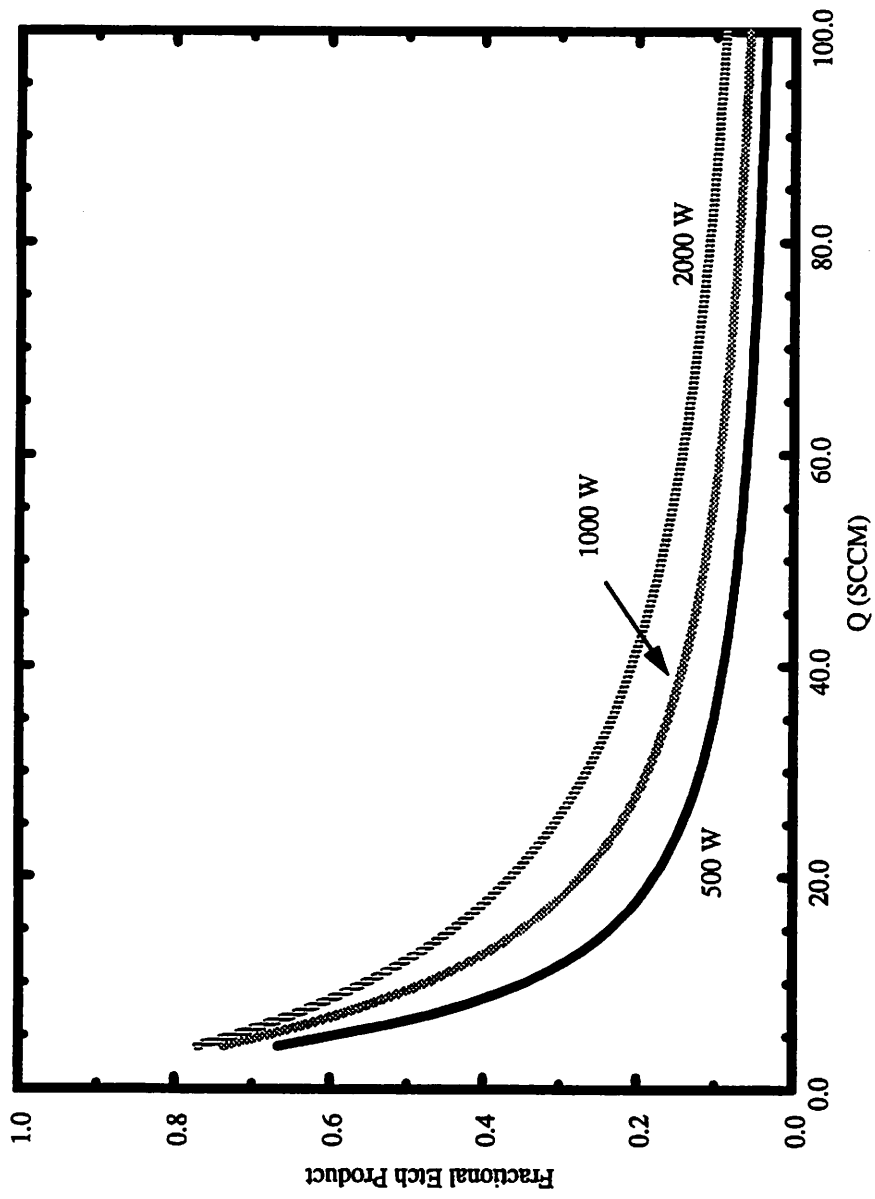


Figure 3. Fractional etch product vs. flowrate, nonreactive wall case. conditions the same as Fig. 2.

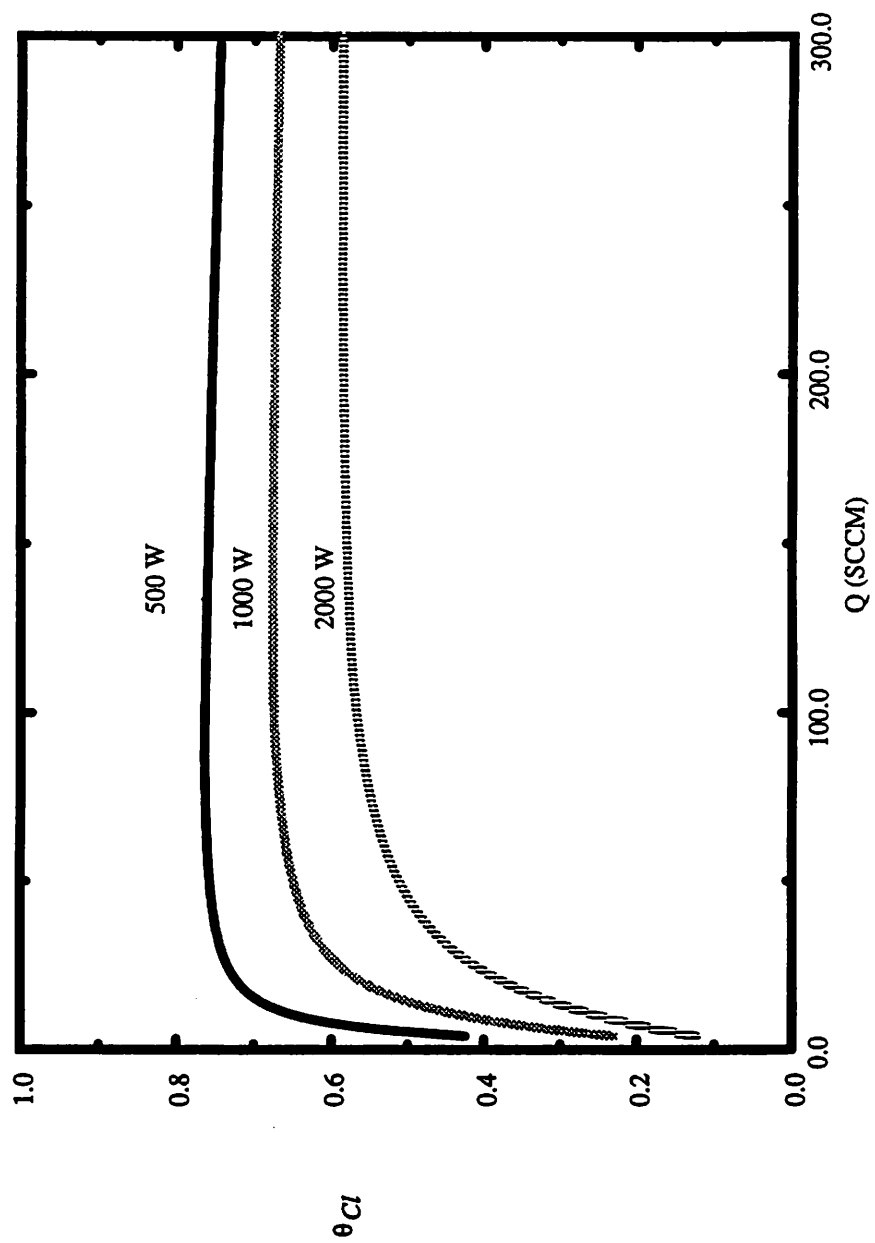


Figure 4. Fractional surface coverage  $\theta_{Cl}$  vs. flowrate, nonreactive wall case.

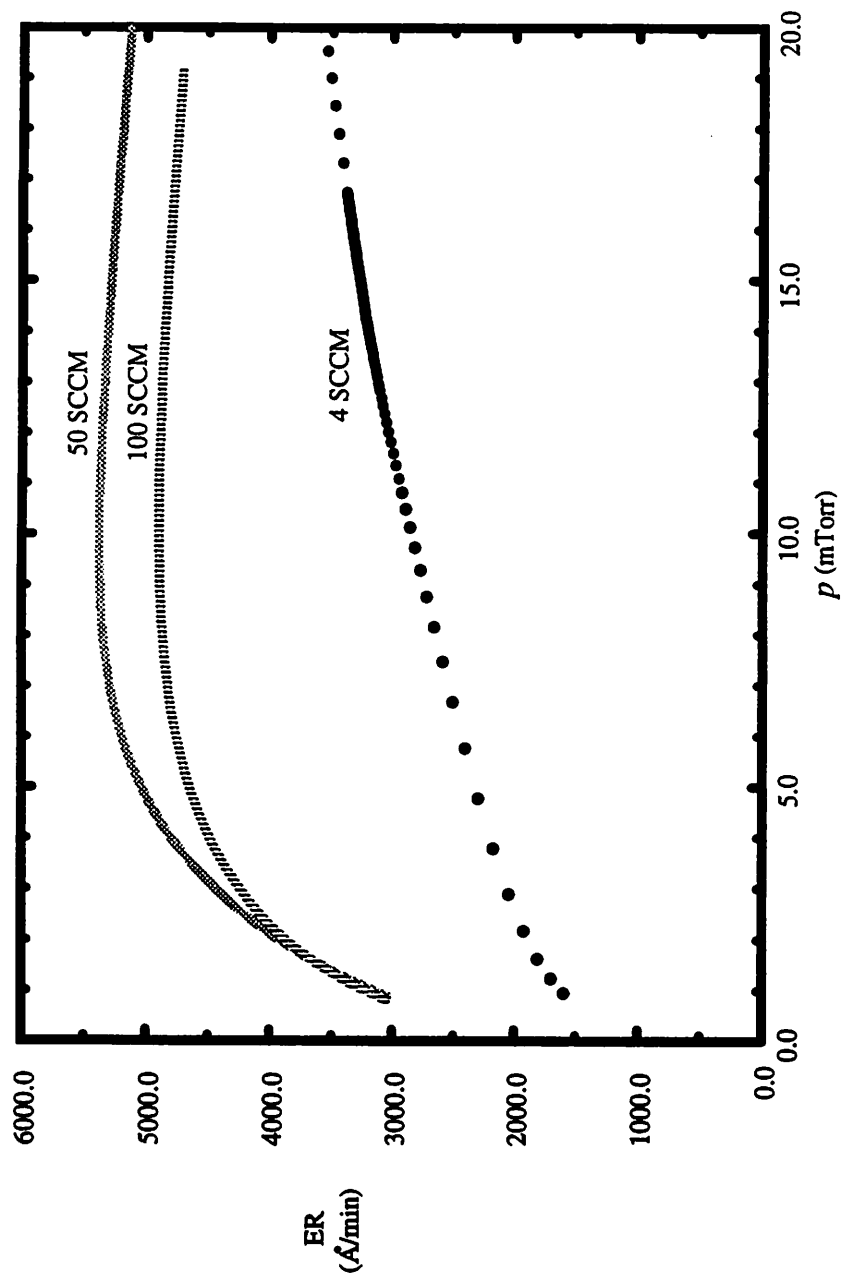


Figure 5. Etch rate vs. pressure, with flowrate as a parameter; nonreactive wall case, coil power = 1000 W.

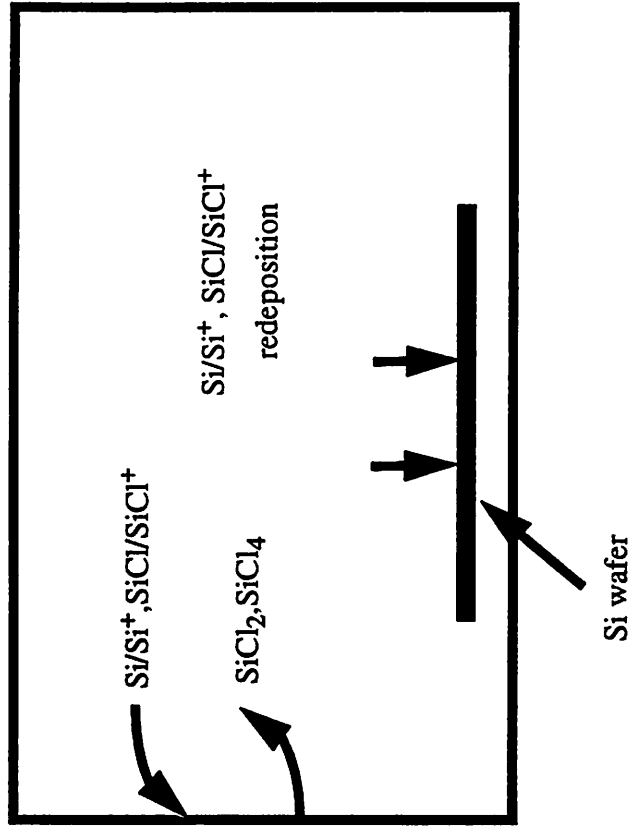


Figure 6. Schematic representation of assumptions used in the reactive wall case.

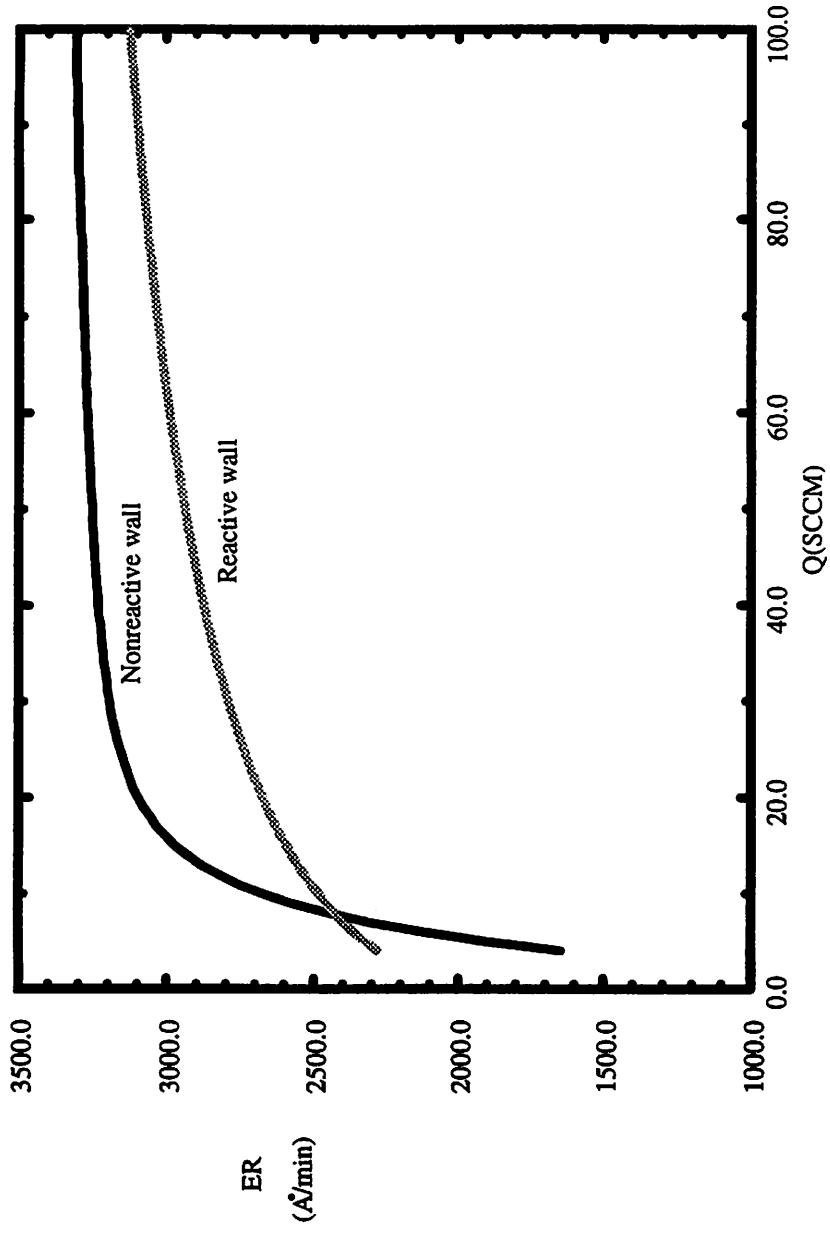


Figure 7. Comparison of etch rate vs. flowrate for nonreactive and reactive walls.

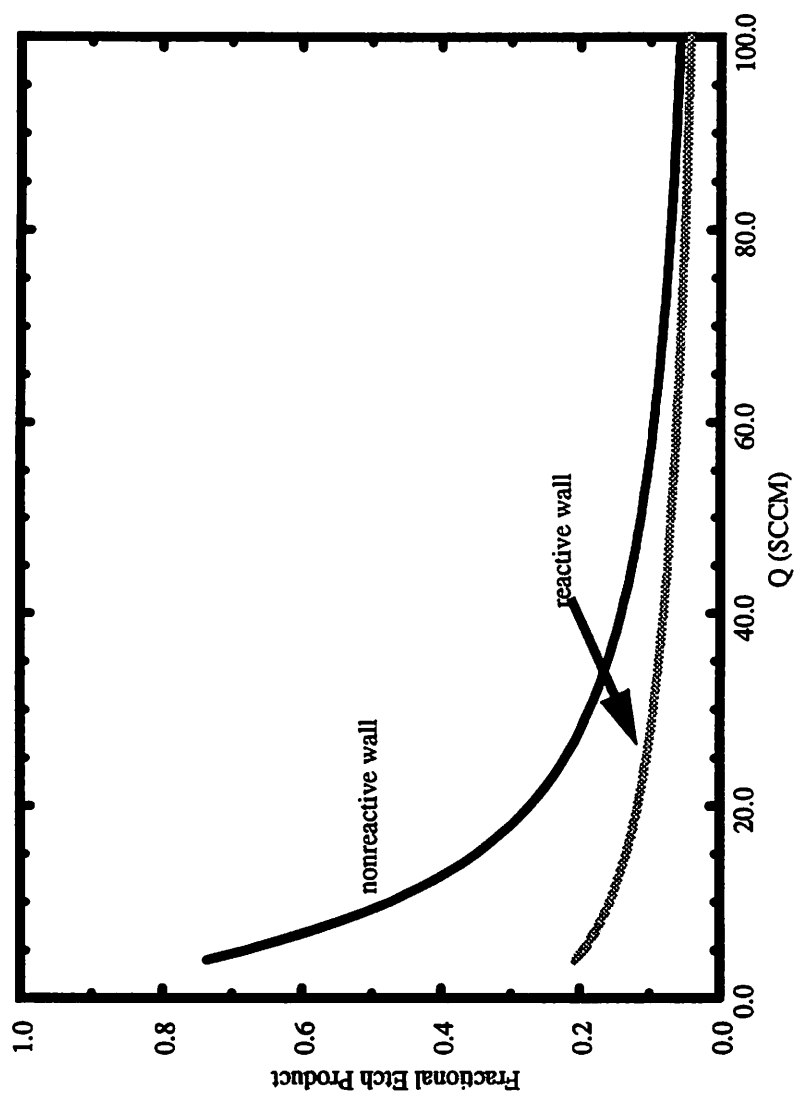


Figure 8. Comparison of the fractional etch product vs. flowrate for nonreactive and reactive walls.

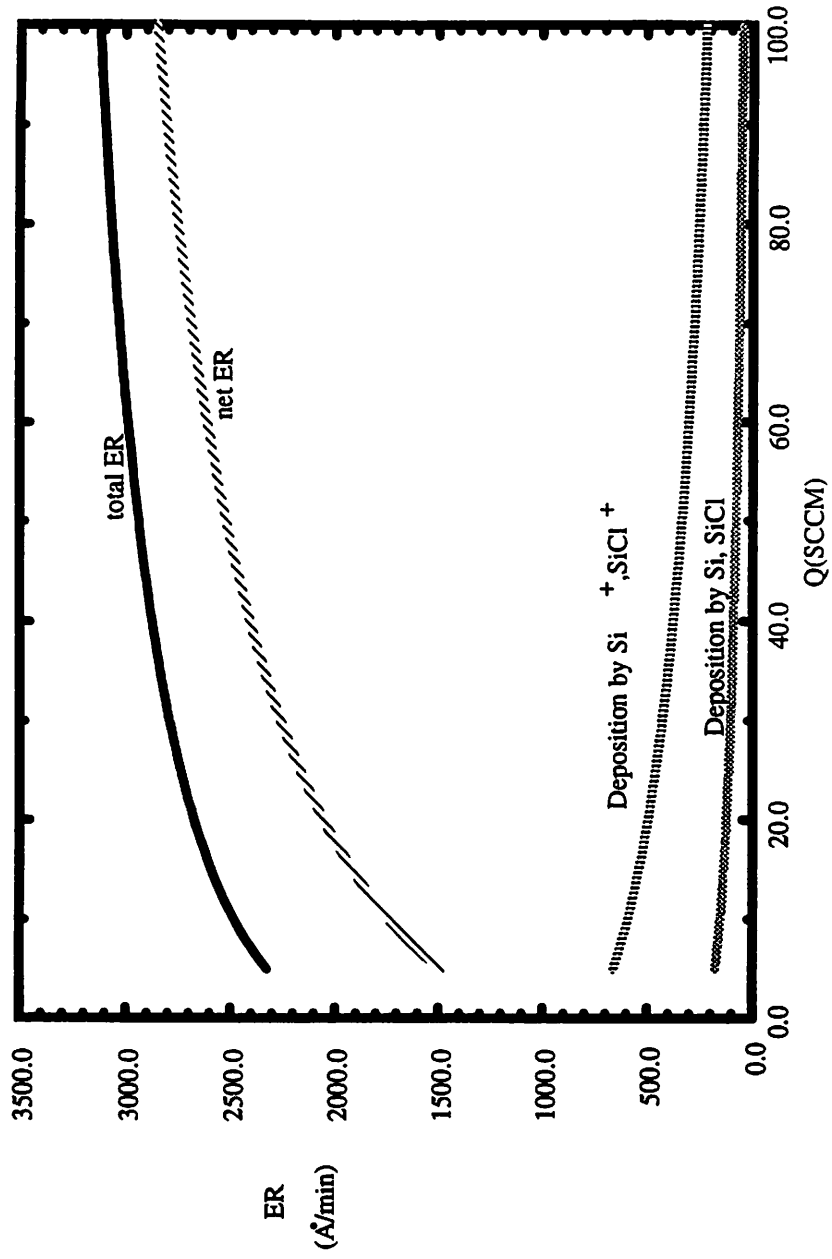


Figure 9. Etch rates and deposition rates of neutrals and ions vs. flowrate for the reactive wall.

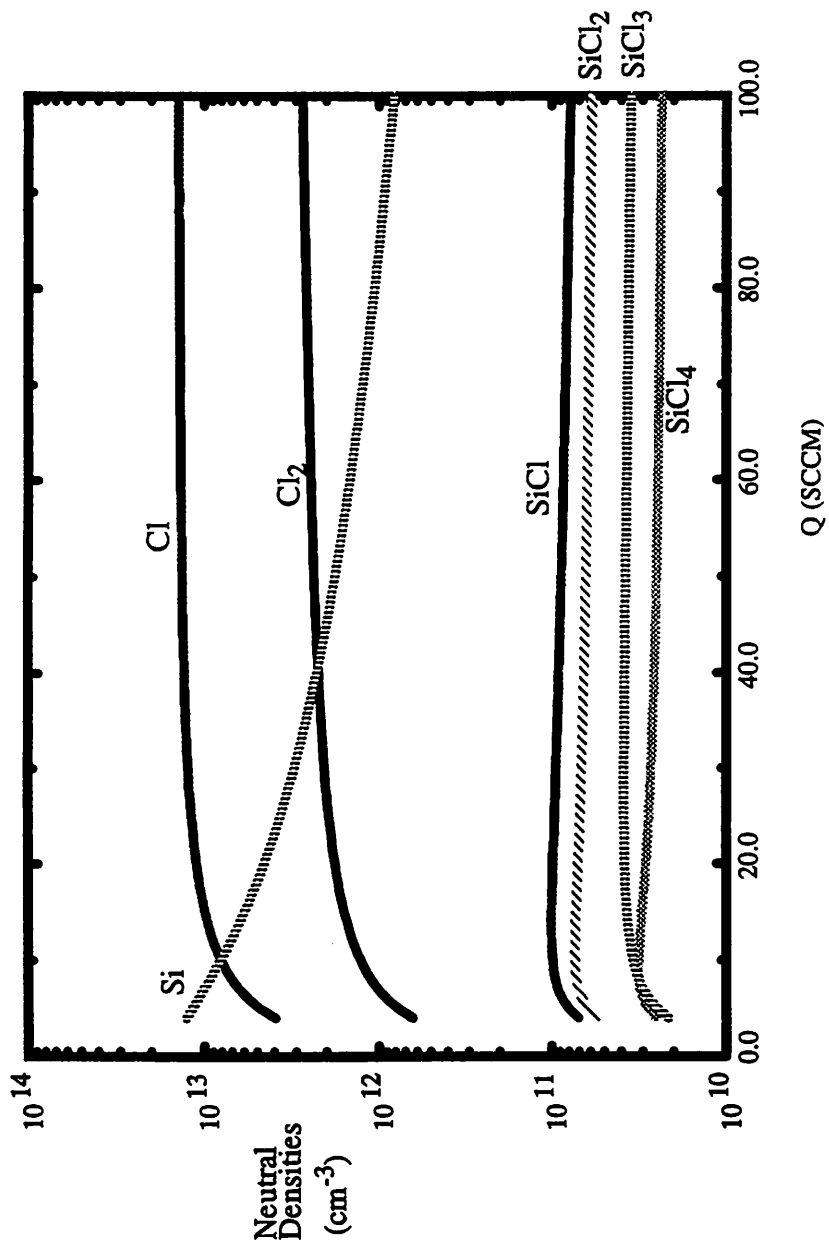


Figure 10a. Neutral densities vs. flowrate at  $p = 1$  mTorr and coil power = 1000 W for the nonreactive wall.

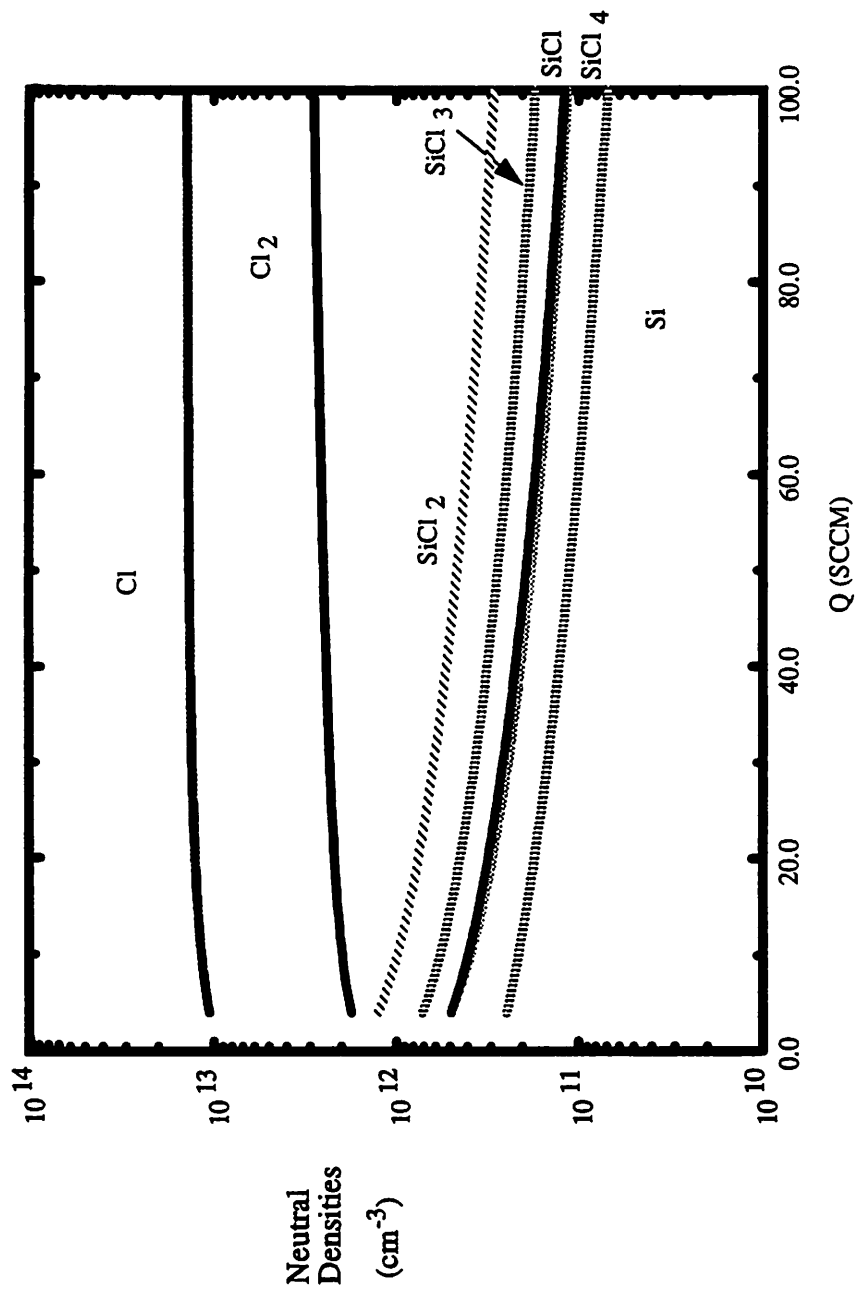


Figure 10b. Neutral densities vs. flowrate at  $p = 1$  mTorr and coil power = 1000 W for the reactive wall.

## References

1. Tsujimoto, K., T. Kumihashi, and S. Tachi, *Appl. Phys. Lett.*, **63**, 1915, (1993).
2. Gray, D. C., V. Homindra, and H. H. Sawin, *J. vac. Sci. Technol.*, **A12** (2), 354, 1994.
3. Dalton, T. J. and H. H. Sawin, presentation at the 41st Symposium of the American Vacuum Society, Denver, CO, 1994.
4. Lee, C., D. B. Graves, M. A. Lieberman, and D. W. Hess, *J. Electrochem. Soc.* **141**(6), 1994.
5. Lee, C. and Lieberman, M. A., to be published in *J. Vac. Sci. Technol. A*.
6. Nakano, T. and H. Sugai, *J. Phys. D. (Appl. Phys.)*, **26**, 1909, (1993).
7. Fisher, E. R. and P. B. Armentrout, *J. Phys. Chem.*, **95**, 4765 (1991).
8. Hayashi, M., in *Swarm Studies and Inelastic Electron-Molecule Collisions*, L. C. Pitchford, B. V. McKoy, A. Chutjian, and S. Trajmar, eds., Springer, New York, 1987.
9. Coburn, J. W., *J. Vac. Sci. Technol. B* **12** (3), 1384, (1994).
10. Hayes, T. R., R. J. Shul, F. A. Baiocchi et al., *J. Chem. Phys.*, **89**, 4035, (1988).
11. Shul, R. J., T. R. Hayes, R. C. Wetzal et al., *J. Chem. Phys.*, **89**, 4042, (1988).
12. Shul, R. J., R. S. Freund, and R. C. Wetzal, *Phys. Rev. A*, **41**, 5856, (1990).
13. Winstead, C., H. P. Pritchard, and V. McKoy, Quarterly Report to Sematech, Inc., Electron Collision Data for Plasma Modelling, May 31, 1994.
14. Freund, R. S., R. C. Wetzal, R. J. Shul, and T. R. Hayes, *Phys. Rev. A*, **41**, 3575, (1990).
15. Gray, D. C., I. Tepermeister, and H. H. Sawin, *J. Vac. Sci. Technol. B* **11**(4), 1243, 1993.
16. Bailey, A. D. III, M. C. M. van de Sanden, J. A. Gregus, and R. A. Gottscho, submitted to *J. Vac. Sci. Technol. A*.
17. Ono K., M. Tuda, K. Nishikawa, T. Oomori, and K. Namba, *Jpn. J. Appl. Phys.*, **33**, 4424, (1994).
18. Winters, H. W. and J. W. Coburn, *Surf. Sci. Rep.*, **14**, 269, (1992).
19. Gerlach-Meyer, U., *Surf. Sci.*, **103**, 524, (1981).
20. Steinbruchel, C., *Appl. Phys. Lett.*, **55**, 1960, (1989).
21. Barone, M. E. and D. B. Graves, to be published in *J. Appl. Phys.*
22. Mayer, T. M. and R. A. Barker, *J. Vac. Sci. Technol.*, **21**(3), 757, (1982).

23. Barker, R. A., T. M. Mayer, and W. C. Pearson, *J. Vac. Sci. Technol.*, **B 1**(1), 37, (1983).
24. Cheng, C. C., K. V. Guinn, V. M. Donnelly, and I. P. Herman, *J. Vac. Sci. Technol. A* **12**(5), 2630, (1994).
25. Flaum, H. C., D. J. D. Sullivan, and A. C. Kummel, *J. Phys. Chem.*, **98**, 1719, 1994.
26. Rossen, R. A. and H. H. Sawin, *J. Vac. Sci. Technol. A* **5**(4), 1595, (1987).